Investigation of the side scattering from a laser-produced plasma at the fundamental frequency

N. E. Andreev, V. L. Artsimovich, Yu. S. Kas'yanov, and V. T. Tikhonchuk

Institute of General Physics of the Academy of Sciences of the USSR

The spatial, temporal, and spectral characteristics of lateral scattering from a laser-produced plasma near the frequency of the warming radiation was studied in experiments on the interaction of the first or second harmonic of neodymium-laser radiation with flat aluminum targets. Two regimes of nonlinear interaction of the laser radiation with the plasma were observed: the regime of generation of narrowly directed ion jets and the regime of self-focusing of the laser beam. When the target was irradiated with the second harmonic of the neodymium laser the first regime was observed for radiation flux densities $q \sim 2 \cdot 10^{14}$–10^{15} W/cm^2 and the second regime was observed for flux densities $q \sim 10^{15}$ W/cm^2. In the experiments with the first harmonic the characteristic thresholds for the appearance of these regimes is approximately two to three times lower. Possible mechanisms for the production of jets and the reasons for the strong lateral scattering are discussed.

1. INTRODUCTION

In experiments on laser-driven thermonuclear fusion spatially nonuniform structures of the density and temperature are observed in the plasma corona. The transverse dimensions of these structures are, as a rule, much smaller than the diameter of the heating-radiation beam, and the structures themselves have an elongated shape and are oriented normally to the target or parallel to the axis of the laser beam. Such structures are called jets and filaments, respectively. Jets and filaments were discovered in experiments with spherical and flat targets with laser radiation of moderate and high intensities. They are observed in a wide range of wavelengths of the warming radiation: from the CO_2 laser up to the fourth harmonic of the Nd laser.[1-8] The most widely employed experimental methods for studying filaments and jets in laser-produced plasma are the shadow and schlieren methods, interferometry, and spatiotemporal detection of radiation from the plasma at the harmonic frequencies $2\omega_0$ and $3\omega_0/2$.[9]

In the present work spatially nonuniform plasma structures were investigated by the method of side scattering near the fundamental frequency, which we proposed earlier.[10] Based on an analysis of the results, we propose a model of the formation of nonuniform structures in a laser-produced plasma. In this model the appearance of such structures is connected with the self-focusing of the laser beam in the plasma when the energy flux densities are high and with the production of narrowly directed ion jets when the flux densities are low.

2. EXPERIMENTAL SETUP

The plasma was produced using the laser setup whose optical layout is shown in Fig. 1. The vacuum spatial filter made it possible to improve substantially the divergence of the laser radiation and the distribution of the field in the near zone. The working parameters of the laser radiation at the wavelength $\lambda_0 = 0.53$ μm are as follows: the maximum beam diameter at the system output is equal to 40 mm, the maximum energy is equal to 20 J, the pulse width ≈ 1.5 ns

(at half-height), the radiation contrast $< 10^{-5}$, the radiation spectrum is a single-frequency spectrum, from 40 to 60% of the output energy has a divergence of $\approx 10^{-5}$ rad, the polarization of the radiation is linear, and the degree of polarization $< 10^{-2}$. The parameters of the laser radiation at $\lambda_0 = 1.06$ μm are as follows: the pulse width is equal to 2 ns, the maximum energy is equal to 50 J, and the diameter of the focusing spot is ≈ 25–30 μm.[11]

The radiation at the first or second harmonic of the neodymium laser was focused with a single lens of focal length $f = 300$ mm on the surface of a flat aluminum target placed in the vacuum chamber. The following were recorded at an angle $\approx 90°$ to the axis of the laser beam and the normal to the target (i.e., in the case of oblique incidence in a direction perpendicular to the plane of incidence): the spatial region of scattering (channel I in Fig. 2); the spatiotemporal structure (channel II); and, the spectrotemporal structure (channel III). The magnification of the optical system was equal to $\approx 30^\times$. The spatial, temporal, and spectral resolutions were equal to 5 μm, 50 ps, and 0.1 nm, respectively. A Dove prism was inserted directly in front of the monochromator (channel III in Fig. 2); this prism made it possible to
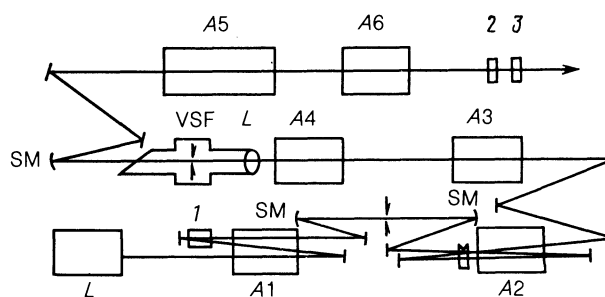

FIG. 1. Optical layout of the laser setup: L—single-frequency neodymium-glass laser; A 1–A 6—amplifiers; VSF—vacuum spatial filter; SM—spherical mirror; LS—lens; 1—two-pass Pockels cell; 2—KDP crystal; 3—SZS-21 filter.
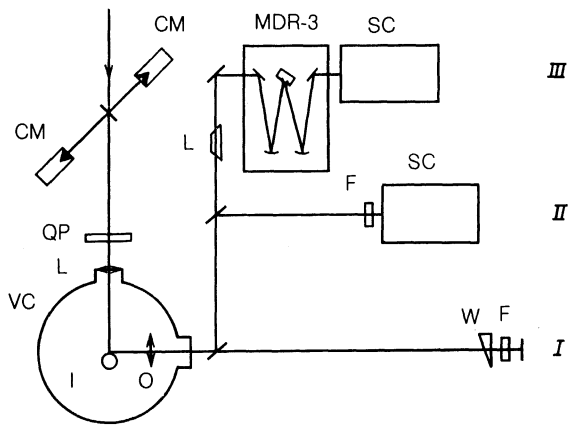
FIG. 2. Experimental arrangement: VC—vacuum chamber; T—target; L—lens; QP—quartz plate; CM—calorimeter; O—Gelios-44 objective; W—Iceland-spar wedge; F—color and neutral light filters; SC—streak camera; P—Dove prism; MDR-3—monochromator.
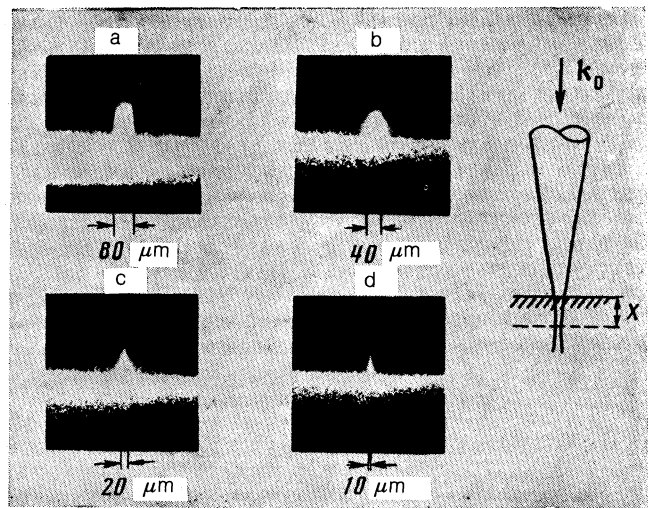

FIG. 3. Lateral scattering for different positions of the caustic of the laser radiation relative to the plane of the target: a) $x = 0.9$ mm; b) $x = 0.7$ mm; c) $x = 0.2$ mm; d) $x = 0$. The fluxes $q < 10^{14}$ W/cm^2, the laser beam is incident normally, and $\lambda_0 = 0.53 \, \mu$m.

orient in the required manner the image of the plane of the target relative to the input slit of the monochromator. SZS–21 and ZhS–17 color filters (transmission bandwidth ≈ 80 nm) were used to reduce the effect of the characteristic thermal radiation of the plasma near $\lambda_0 = 0.53 \, \mu$m when the spatial structure was recorded in the channels I and II.

The parameters of the side scattering were studied for two orientations of the linear polarization of the laser radiation: perpendicular and parallel to the scattering plane containing the axis of the laser beam and the observation axis. The polarization plane of the laser beam was rotated by 90° with the help of a quartz plate QP (Fig. 2). An image of the scattering region was recorded on photographic film in two orthogonal polarizations with the help of an Iceland-spar prism K: parallel and perpendicular to the polarization plane of the laser radiation.

3. EXPERIMENTAL RESULTS

3.1. Spatial structure of scattering

As shown earlier,[10] at moderate flux densities of the second harmonic of the neodymium-laser radiation at the target ($q < 10^{14}$ W/cm^2) the side scattering near the fundamental frequency is determined by the Mandel'shtam–Brillouin process (MBS), i.e., by the scattering of laser radiation by thermal ion-sound oscillations in the plasma. The intensity of the radiation scattered at an angle of 90° was equal to 10^{-7}–10^{-9} times the intensity of the warming radiation. Since this process is linear in the intensity, the method of lateral scattering makes it possible to study the structure of the laser field near the target. As an illustration Fig. 3 shows a photograph of the region of scattering at the wavelength $\lambda_0 = 0.53 \, \mu$m for different positions of the caustic of the laser beam relative to the target plane. The minimum diameter of the caustic is equal to 10–12 μm, which is close to the 12–14 μm diameter of the minimum focusing spot, measured by the mirror-wedge method.

For higher laser-radiation flux densities at the frequencies of both the first and second harmonics two significantly different scattering regimes arise.

High-flux regime. Figure 4 shows a photograph of the scattering region ($\lambda_0 = 0.53 \, \mu$m) in two polarizations in the

case of maximum flux density $q \approx 10^{15}$ W/cm^2. The laser radiation is polarized perpendicular to the scattering plane. The scattered radiation is appreciably depolarized and emanates from a small region ("spot") near the surface of the target. In separate experiments the intensity of the "spot" is several orders of magnitude higher than the intensity of scattering from the caustic at moderate fluxes.

Intermediate-flux regime. In this case ($\lambda_0 = 0.53 \, \mu$m) the size of the spot on the surface of the target is equal to 20–30 μm and the scattering is characterized by the appearance of a strongly elongated (up to 200–300 μm) and narrow (5–10 μm) nonuniform structure, previously observed in ex-
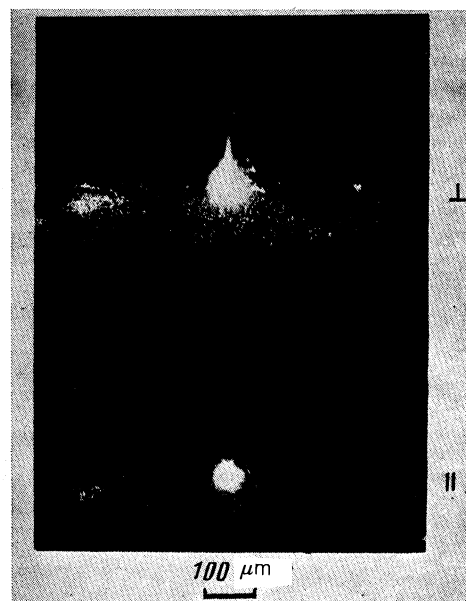

FIG. 4. Photograph of the region of scattering in two orthogonal polarizations: parallel ($\parallel$) and perpendicular ($\perp$) to the scattering plane. The radiation is incident normally, $q \approx 10^{15}$ W/cm^2, and $\lambda_0 = 0.53 \, \mu$m. The polarization plane of the laser radiation is perpendicular to the scattering plane.
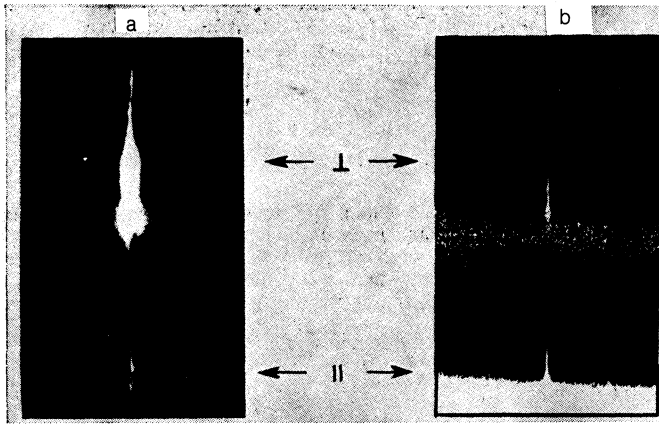
FIG. 5. Photograph of the scattering region in two orthogonal polarizations. The polarization plane of the laser radiation is perpendicular (a) and parallel (b) to the scattering plane. The radiation is incident normally, $q = 2 \cdot 10^{14}$ W/cm^2, and $\lambda_0 = 0.53$ μm.

periments at the first harmonic frequency of the neodymium laser.[11]

Figure 5 shows characteristic photographs of the scattering, obtained by irradiating the targets with the second harmonic of the neodymium laser, for two orientations of the polarization of the laser radiation. In the case when the polarization plane is perpendicular to the scattering plane, the scattering intensity is significantly higher than the intensity of Mandel'shtam-Brillouin scattering (Fig. 5a⊥). The scattered radiation with the "forbidden" polarization (Fig. 5a∥) is much weaker and is apparently due to the depolarization of radiation in the optical elements of the detection scheme as well as to the imprecise alignment of the optical axis of the Iceland-spar prism relative to the scattering plane. The possible angular misalignment of 2–3° between the optical axis of the prism and the scattering plane explains the observed ratio of the intensities.

If the polarization plane of the warming radiation lies in the scattering plane (Fig. 5b), then the intensity of the scattering in both channels is approximately the same and signif-

icantly weaker than the scattering in the first case (Fig. 5a⊥). The ratio of the scattering intensities in the first and second cases is explained well by the angular dependence of the cross section of the Mandel'shtam–Brillouin process when the aperture of the recording system is taken into account.

The results of the investigation of the spatiotemporal structure of the scattering in the case when the targets are irradiated with the second harmonic of a neodymium laser demonstrate that the behavior of the scattering regions as a function of time is analogous to the behavior we observed earlier in the case when the targets are irradiated at a wavelength $\lambda_0 = 1.06$ μm.[11] The scattering arises first from regions of the plasma near the surface of the target and moves toward the laser radiation with velocity $\geqslant 10^8$ cm/s. Intense scattering is observed in the leading edge of the laser pulse and pulsates in time. The spatiotemporal pulsations of the scattering are more pronounced in the case of irradiation at the wavelength $\lambda_0 = 1.06$ μm.

For oblique incidence ($\theta = 20°$) of laser radiation with wavelength $\lambda_0 = 1.06$ μm on the target two regions of intense scattering are observed. One region, corresponding to scattering from the caustic, has an elongated shape and is oriented along the axis of the laser beam. The other region, representing scattering from the jet, is oriented virtually normally to the surface (Fig. 6a). In experiments with $\lambda_0 = 0.53$ μm the intensity of scattering from the jet is significantly weaker.

3.2. Spectral distribution of the lateral scattering

In the case of normal incidence the appearance of a fine spatial structure in the lateral scattering is accompanied by a change in the spectrum of the scattering. In experiments with $\lambda_0 = 0.53$ μm there arises, together with two Mandel'shtam–Brillouin components, a third intense line in the short-wavelength region of the spectrum (Fig. 7). At lower radiation intensities this line practically coincides with the anti-Stokes component of the Mandel'shtam–Brillouin scattering (Fig. 7b), and then, as the radiation flux density is increased, it shifts into the shorter wavelength region (Fig. 7a). An analogous dependence of the spectrum of the lateral scattering on the flux density is observed in experiments at
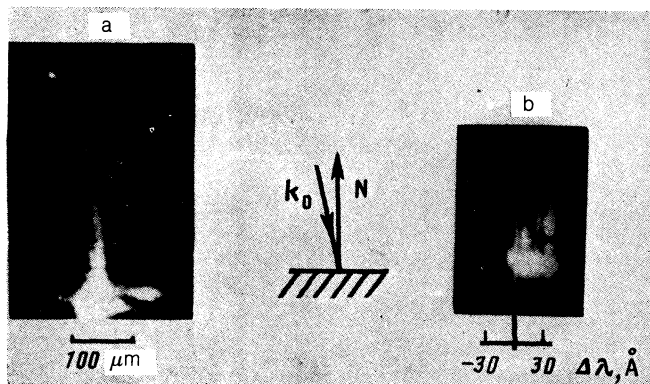

FIG. 6. Photograph of the region of scattering with oblique incidence ($\theta = 20°$) of the laser radiation on the target, $\lambda_0 = 1.06$ μm (a), and the scattering spectrum from the region of the jet (b); $\Delta\lambda = \lambda' - \lambda_0$, where λ' is the wavelength of the scattered radiation.
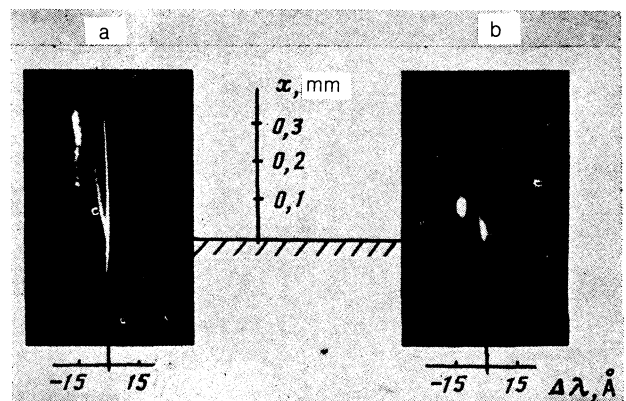

FIG. 7. The lateral-scattering spectrum for normal incidence of the laser radiation ($\lambda_0 = 0.53$ μm) for two flux densities, q_1 (a) and q_2 (b), $q_1 > q_2$.
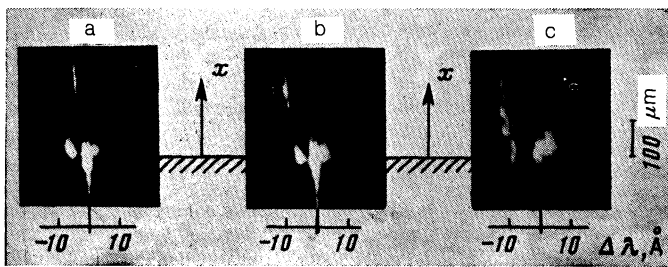
FIG. 8. The lateral-scattering spectra for normal incidence of the laser radiation ($\lambda_0 = 1.06 \mu$m) for different energy flux densities q (W/cm^2): $2 \cdot 10^{13}$ (a), $4 \cdot 10^{13}$ (b), and 10^{14} (c).

the wavelength $\lambda_0 = 1.06 \mu$m (Fig. 8). The appearance of long-wavelength components is connected with scattering of laser radiation, reflected from the critical surface, by the ion-sound fluctuations of the density in the rarefied plasma.

For oblique incidence of the laser radiation the spectral distribution is substantially different in the two scattering regions indicated above. The spectrum from the region of the caustic is analogous to the spectrum of scattering at normal incidence and moderate fluxes: two lines—Mandel'shtam–Brilluoin components, shifted in the short-wavelength direction, and the intensity of the first (Stokes) component is, as a rule, higher than that of the anti-Stokes component. The spectrum of the scattering from the region of the jet is broadened and shifted into the long-wavelength region (Fig. 6b).

Figure 9 shows a temporal scan of the spectrum of the lateral scattering for normal incidence of the warming radiation with wavelength $\lambda_0 = 1.06 \mu$m. The intensities of the first component (Stokes scattering) and of the additional line pulsate in time and often exist seemingly in antiphase. An analogous, but less pronounced, temporal structure of the spectrum also occurs in experiments with the wavelength $\lambda_0 = 0.53 \mu$m.

3.3. Experimental results

Summarizing what we have said above, we shall present the main results of the experimental investigation of the lateral scattering.
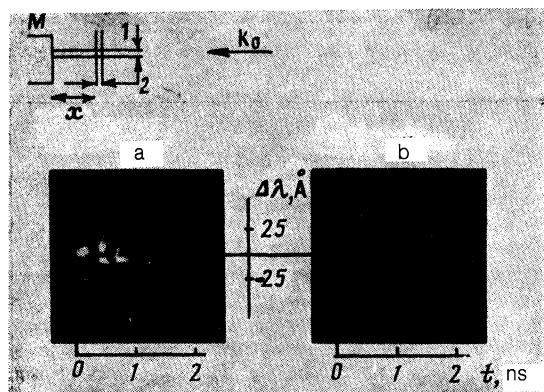

FIG. 9. Time scans of the side-scattering spectrum at different distances from the target: $x = 15 \mu$m (a), $x = 60 \mu$m (b). The radiation is incident normally, $\lambda_0 = 1.06 \mu$m, and $q \geqslant 10^{14}$ W/cm^2. The mutual orientation of the target (T) plane, the input slit of the monochromator (2), and the time-scan slit of the streak-camera (1) are shown at the top of the figure.

1. In experiments with laser radiation flux densities greater than $4 \cdot 10^{13}$ W/cm^2 at a wavelength of $\lambda_0 = 1.06 \mu$m and greater than 10^{14} W/cm^2 at a wavelength $\lambda_0 = 0.53 \mu$m there arises a region of intense scattering—a jet (Fig. 5). This is a narrow region (5–10 μm) extending up to 300 μm along the normal to the target.

2. The velocity of the region of intense scattering from the target is greater than 10^8 cm/s, and the scattering itself is of a pulsating character with a period of the order of 100 ps.

3. The appearance of a moving region of strong lateral scattering is accompanied by a severalfold increase in the coefficient of reflection backwards into the lens and can reach values of the order of 5% for experiments at the wavelength $\lambda_0 = 1.06 \mu$m.

4. The lateral scattering from the jet is 10^2–10^3 times stronger than the lateral scattering from the region of the caustic in the absence of a jet.

5. In the case of normal incidence the appearance of a jet is accompanied by the appearance of an additional line, shifted in the short-wavelength direction, in the scattering spectrum. The magnitude of the shift is always greater than or equal to that of the anti-Stokes component of spontaneous Mandel'shtam–Brillouin scattering and increases as the flux density of the laser radiation increases (Figs. 7 and 8).

6. In the case of oblique incidence ($\theta = 20°$) the spectrum of scattering by the jet is broadened and shifted into the long-wavelength region (Fig. 6), while the scattering spectrum from the region of the caustic is analogous to that from the region of the caustic in the case of normal incidence and moderate fluxes.

7. At high flux densities ($q \sim 10^{15}$ W/cm^2 for the wavelength $\lambda_0 = 0.53 \mu$m and $q \geqslant 5 \cdot 10^{14}$ W/cm^2 for $\lambda_0 = 1.06 \mu$m), strong depolarized scattering from a small region—a spot—near the surface of the target arises (Fig. 4).

4. DISCUSSION

The data presented above indicate that there exist three qualitatively different regimes of interaction of laser radiation with plasma.

1. The regime of moderate fluxes ($q \leqslant 10^{14}$ W/cm^2 for $\lambda_0 = 0.53 \mu$m) is characterized by the absence of nonlinear effects in the lateral scattering. In Ref. 10 this is interpreted as spontaneous Mandel'shtam–Brillouin scattering.

2. The regime of intermediate fluxes is characterized by the presence of localized moving regions in the lateral scattering and a more complicated structure of the scattering spectrum.

3. The regime of high fluxes ($q \geqslant 10^{15}$ W/cm^2 for $\lambda_0 = 0.53 \mu$m) is characterized by the presence of a bright "spot" source of wide-angle depolarized scattering in a dense plasma.

4.1. Regime of high radiation fluxes

We associate this regime with self-focusing of the laser beam in its path from the rarefied plasma to the region of absorption. This conclusion is based on the following:

the observed threshold is qualitatively (with respect to the dependence on the parameters) equal to the threshold of self-focusing of a laser beam in the corona plasma and is quantitatively close to it;

the region of the focus (bright "spot") lies in the dense

Andreev *et al.*   493

plasma (in a neighborhood of the region of absorption) and is practically stationary;

intense scattering from the focus is a characteristic of self-focusing and is associated with the heating of the plasma and with significant deformation of the density profile.

To justify this model we shall examine the conditions of self-focusing of a laser beam in a plasma. The profile of the laser beam in the experiments under discussion is close to Gaussian and it does not contain any small-scale nonuniformities. For this reason the breakup of the beam into filaments (small-scale self-focusing–filamentation[12]) does not occur, but rather the beam as a whole is self-focused.

In these experiments self-focusing could be due either to striction or thermal mechanisms of nonlinearity. The electron mean-free path in the region of critical density n_c

$$\lambda_{ei}^{\bullet} = V_{Te}/v_{ei}^{\bullet},$$

[where V_{Te} is the thermal velocity of the electrons and v_{ei}^* is the electron-ion collision frequency at density $n_e = n_c$, under the conditions of the experiment (the electron temperature is $T_e \approx 0.5$ keV, the ion charge is $Z \approx 10$ (aluminum target), and $n_c = 4 \cdot 10^{21}$ cm^{-3} $d \geqslant 10 \mu$m)] is equal to about 0.2 μm, which is significantly less than the diameter of the laser beam on the surface of the target. For this reason self-focusing at the initial stage is apparently caused by the non-uniform heating of the plasma by the laser beam.[12-14] As the beam is compressed and the plasma heated, however, the electrostriction effect can become more important. The length L_t, at which the thermal self-focusing of a light beam with a Gaussian distribution of intensity occurs in a uniform plasma, is determined by the expression

$$L_t \approx \alpha_t \lambda_{ei} \left(\frac{n_c}{n_e}\right)^{1/2} \frac{V_{Te}}{V_E},$$

where α_t is a numerical factor, $\lambda_{ei} = V_{Te}/v_{ei}$ is the mean free path of an electron in a plasma with density n_e and collision frequency v_{ei}, and V_E is the speed of oscillations of the electrons in the field of the laser radiation. In the case of striction nonlinearity the expression for the self-focusing length has the form

$$L_p = \alpha_p d \left(\frac{n_c}{n_e}\right)^{1/2} \frac{V_{Te}}{V_E},$$

where α_p is a numerical factor. In the expressions for L_p and L_t the diffraction effects were neglected, since in a nonuniform plasma self-focusing is possible if the self-focusing length does not exceed the spatial size of the nonuniformity of the plasma density L_N, which is comparable to the diameter of the laser beam and significantly less than the diffraction length d^2/λ_0. The formulas for L_p and L_t were derived by different authors in a number of works,[13-15] in which, however, the numerical values of the coefficients α_p and α_t differ by several times. We shall follow below the formulas of Ref. 14, setting for definiteness $n_e/n_c \approx 0.5$, bearing in mind the fact that in a nonuniform plasma these formulas must be regarded as only approximate. In terms of dimensional quantities, according to Ref. 14, we have

$$L_t = (\lambda_0/\pi) \gamma_{T_2}^{-1/2}, \qquad L_p = (\pi d/0.56) \gamma_p^{-1/2},$$

where

$$\gamma_{T_2} = 0.23 \cdot 10^{-7} q_0 Z^2 T_e^{-5} (Z+0.24)/(1+0.24Z),$$

$$\gamma_p = 1.32 \cdot 10^{-2} \lambda_0^2 q_0 T_e^{-1} Z/(1+Z),$$

q_0 is the flux density in units of 10^{14} W/cm^2, λ_0 is given in μm, and T_e is given in keV. Substitution of the parameters of the experiments at the wavelength $\lambda_0 = 0.53 \mu$m ($T_e = 0.5$ keV, $d = 10 \mu$m, and $q = 10^{15}$ W/cm^2) gives

$$L_t = 10 \mu\text{m}, L_p = 26 \mu\text{m}.$$

These lengths are comparable to the nonuniformity scale of the plasma density, so that under the conditions studied self-focusing is possible. In our experiments the laser-beam power was maintained constant at $P_0 = \pi q_0 d^2/4 \approx 1$ GW. For this reason, when q_0 decreased d increased and, correspondingly, L_t and L_p increased; in addition, because of the nonuniformity of the electron density, self-focusing apparently did not occur before the laser beam was reflected.

As one can see from the expressions presented for L_t and L_p, the striction mechanism of self-focusing in the plasma becomes much more important for radiation with the wavelength $\lambda_0 = 1.06 \mu$m, and it apparently determines the threshold of self-focusing, which in this case is approximately two times lower than the threshold of self-focusing for radiation with $\lambda_0 = 0.53 \mu$m.

Thus the assumption of self-focusing of the laser beam in our experiments qualitatively agrees with the existing theoretical ideas.

4.2. Regime of intermediate energy fluxes

The arguments and estimates presented above give grounds for concluding that in the regime of intermediate fluxes ($q \approx 10^{14}$–10^{15} W/cm^2) self-focusing of the laser beam does not occur, but rather that the observed nonlinear lateral scattering is caused by other physical processes.

The intense scattering arising in this case in a narrow region, extending along the normal to the target and moving with velocity $V \geqslant 10^8$ cm/s, pulsating in time and accompanied by the appearance of an additional line, shifted in the short-wavelength direction in the lateral-scattering spectrum, suggests that in a laser-produced plasma a narrow beam of accelerated ions is produced at intermediate fluxes. In contrast to other experiments,[4,8] where plasma jets were observed at the trailing edge or after the termination of the laser pulse, in our case the ion beam is produced on the leading edge of the laser pulse and it has a short duration ($\leqslant 100$ ps).

The supersonic flux of ions in the expanding laser plasma excites ion-sound waves propagating in the same direction, particularly waves from which the observed scattering of laser radiation occurs. This could be the reason for the significant increase in the scattering intensity. We note that heating of the plasma and, possibly, dragging of the plasma by the ion beam results in an increase of the frequency shift of the excited line relative to the shift of the anti-Stokes satellite of Mandel'shtam–Brillouin scattering arising in the plasma outside the region of the ion beam.

We shall estimate the ion-beam density required in order for ion-sound instability to arise in the surrounding plasma. We assume that the spread in the velocities in the ion beam δU_b is not too small: $\delta U_b > U_b (n_b/n_i)^{1/2}$, where U_b is

the velocity of fast ions in the jet relative to the plasma, n_b is the density of the fast ions, n_i is the density of ions in the surrounding plasma, and $n_i \gg n_b$. Then buildup of ion-sound waves with wave vector k occurs in the kinetic regime and the instability increment is given by the expression[16]

$$\Gamma(k) \approx \left(\frac{\pi}{8}\right)^{1/2} \frac{n_b}{n_i} \frac{k U V_s^3}{(\delta U_b)^3} - \left(\frac{\pi}{8}\right)^{1/2} \frac{k V_s^2}{V_{Te}}$$

$$= (P-1)\left(\frac{\pi}{8}\right)^{1/2} \frac{k V_s^2}{V_{Te}},$$

where V_s is the velocity of sound, the first term is due to the buildup of ion-sound waves by the ion beam, and the second term is due to the attenuation of the ion-sound waves by the electrons. From the condition $\Gamma \geq 0$ ($P \geq 1$) we obtain

$$n_b/n_i \geq (\delta U_b)^3/U_b V_{Te} V_s,$$

which corresponds to $n_b/n_i \geq 0.1$, if it is assumed that $\delta U_b \approx 3V_s$, $U_b \approx 10V_s$, and $V_{Te} \approx 100V_s$. The estimated ion density in the region of scattering is $n_i \approx 10^{19}$ cm^{-3}. Correspondingly, we obtain $n_b \geq 10^{18}$ cm^{-3}.

We shall determine, starting from the generally accepted mechanism of nonlinear saturation of ion-sound turbulence (induced scattering of sound by ions in the plasma), the spectral density W_s of ion-sound waves in the region where the instability builds up. Using the results of Refs. 17–19 we have

$$\frac{W_s}{T_e} \approx P \frac{\omega_{Li}}{\omega_{Le}} \frac{Z T_e}{T_i} \frac{n_e}{k^3} \ln \frac{1}{k r_D}, \qquad (1)$$

where ω_{Li} and ω_{Le} are the Langmuir frequencies of the ions and electrons of the plasma and r_D is the Debye radius. For the conditions of the experiment the estimate following from the formula (1) for $k = \sqrt{2} k_0$ (lateral scattering) with $P \approx 1$ gives $W_s/T_e \approx 10^3$–10^4, i.e., the Mandel'shtam–Brillouin scattering from the region of the ion beam can be three to four orders of magnitude stronger than the spontaneous scattering. This agrees with the estimates of the intensity of the scattering observed in the experiment. As the wave number k decreases, i.e., the wavelength of the laser radiation is increased, the ratio of the turbulence level to the thermal level increases. This also agrees with the data from the experiment where the intensity of the anti-Stokes scattering obtained using the first harmonic of the Nd-laser radiation is higher than for the second harmonic.

We note that in the regime of intermediate fluxes the ratio of the intensities of the lines in the Stokes–anti-Stokes doublet of the Mandel'shtam–Brillouin scattering, arising from regions of the plasma outside the ion beam, decreases. This indicates that the lateral scattering changes from spontaneous to induced. This agrees with the theoretical estimates of the gain of induced Mandel'shtam–Brillouin lateral scattering[20]

$$\varkappa \approx \frac{V_E^2}{V_{Te}^2} \frac{d}{\lambda_0} \frac{\omega_s}{\Gamma_s}.$$

Here $(V_E/V_{Te})^2 \approx 0.01$, d is the size of the region of amplification, and $\omega_s/\Gamma_s \approx 10$ is the ratio of the frequency of sound to the damping decrement of the sound. The fact that $\varkappa$ increases as λ_0 decreases agrees with the experimental data on

the ratio of the intensities of the components of the doublet (Mandel'shtam–Brillouin scattering) at the frequencies of the first and second harmonics of the Nd laser.

4.3. On the mechanisms of the production of a beam of accelerated ions in the plasma

The formation of a beam of fast ions could be connected either with the resonant acceleration of ions in the region of critical density[20] or with the acceleration of the ions as the plasma expands into the vacuum in the presence of a beam of fast electrons in the plasma.[21]

In the first case the ions are accelerated by the ponderomotive force of the field of the Langmuir wave arising upon transformation of the p-polarized component of the laser radiation in the region of critical density. In order for the ions to acquire an energy $E_i > Z T_e$ the amplitude of the field of the plasma wave must be amplified by a nonlinear mechanism. This occurs as a result of aperiodic parametric instability, whose threshold is[20]

$$q_{th} \approx c n_c T_e \frac{L_N}{\lambda_0} \Phi^{-2}(\theta) \left(\frac{\nu_{eff}}{\omega_0}\right)^4 \frac{m_i}{Z m_e}, \qquad (2)$$

where θ is the angle of incidence of the pump wave and $\Phi(\theta)$ is the resonance function[21] characterizing the efficiency of the transformation of laser radiation into the Langmuir wave, and $\nu_{eff} = \max\{\nu_{ei}, \omega_0 (r_d/L_N)^{2/3}\}$.

In accordance with what was said above the inequality $q > q_{th}$ is the condition for the generation of accelerated ions, which, according to Ref. 20, acquire the energy

$$E_i = 30 Z (L_N/\lambda_0)^{2/5} T_e^{4/5}, \qquad (3)$$

where T_e and E_i are measured in keV. The acceleration occurs along the density gradient of the plasma, and the angular spread of the beam of accelerated electrons $\delta\theta \approx (T_i/E_i)^{1/2}$ is very small. The density of the beam of accelerated ions is in principle limited only by the critical value of the density. For this reason, this mechanism can give the fast-ion density required for explaining the data on the scattering of laser radiation ($\approx 10^{18}$ cm^{-3}, which is equal to not more than 1% of the critical density).

The width of the pulse of fast ions is determined by the time over which the profile of the density in the region of the critical density is restructured under the action of strong turbulence and is equal to approximately $L_N/V_s > 10^{-11}$ s, which also agrees with the experimental data.

Thus the possibility of attributing the acceleration of ions to the ponderomotive force is connected with the satisfaction of the condition (2). The function $\Phi(\theta)$ reaches its maximum value $\Phi_{max} \approx 1$ at the angle $\theta_m \approx 0.4 (\lambda_0/L_N)^{1/3}$, which for our conditions is equal to about 6–10°. This value is comparable to the angle $\delta\theta$ of convergence of the rays in the laser beam ($d/f = 0.12$, $\delta\theta \approx 5°$). For normal incidence of first-harmonic radiation, setting $\varphi^2 = 0.1$, we obtain from Eq. (2) the threshold for the acceleration of ions $q_{th} = 10^{14}$ W/cm^2, which agrees with experiment. The threshold is determined by the emission of plasma waves ($\omega_0 (r_d/L_N)^{2/3} > \nu_{ei}$). A transition to the second harmonic increases the threshold (2) by several times owing to the increase in the collision frequency. Increasing the angle of incidence of the laser radiation to $\theta \approx 20°$ also increases the

ion acceleration threshold (2) owing to the sharp decrease of the function $\Phi(\theta)$.

The increase in the threshold (2) with decreasing radiation wavelength and increasing angle of incidence agrees qualitatively with experiment. However the experimentally observed increase in the threshold for the appearance of a jet is not as steep as follows from the formula (2). This gives a basis for suggesting that a second mechanism for the production of fast ions also plays a definite role in our experiments.

According to Ref. 22, where the expansion of a plasma into a vacuum is studied in the case of a two-temperature electron distribution, the formation of fast ions occurs in a rarefied plasma, where the density of the hot electrons n_h is such that their pressure $n_h T_h$ is comparable to that of the surrounding plasma $n_c T_c$. Parametric instabilities in the neighborhood of the critical density could also be a source of hot electrons, but in contrast to the preceding case here both p and s polarized electromagnetic waves can serve as the pump. Efficient acceleration of ions can be expected if the parametric instability occurs under conditions of strong coupling of the waves, i.e., for[23]

$$q > 5 c n_c T_e (m_e Z / m_i)^{1/3}, \qquad (4)$$

which for our parameters is equal to $\approx 10^{14}$ W/cm^2 for the first harmonic of the Nd laser and $\approx 4 \cdot 10^{14}$ W/cm^2 for the second harmonic. The relation (4) is virtually independent of the angle of incidence of the radiation; this agrees with the experiment.

For the second mechanism of generation of fast ions, the fact that the fast ions are narrowly directed requires a special explanation. In our opinion, a jetlike fast-ion production can occur if the current of fast electrons is not compensated by a return current of slow electrons. Because of the small transverse size of the plasma this situation is possible in the experiments being discussed. An uncompensated current of fast electrons leads to the generation of a magnetic field in the corona of the laser-produced plasma, which, in turn, rotates the electrons. The magnetic field is nonuniform—it is equal to zero on the axis of the laser beam and increases toward the periphery. In the process, only the electrons that are moving along the symmetry axis of the system (i.e., along the normal to the target), where the magnetic field is weak, leave the production region. The characteristic transverse size of the beam of fast electrons r_b can be estimated from the condition that the electrons rotate at the edge of the beam in its characteristic magnetic field, whence $r_b \approx c / \omega_h$, where ω_h is the plasma frequency of the beam of fast electrons. If the density of the fast electrons is taken to be $n_h \approx 10^{19}$ cm^{-3} (which is necessary in order to create a beam of ions with $Z = 10$ and density $n_b \approx 10^{18}$ cm^{-3}), then from this estimate we obtain $r_b \approx 2$ μm, which agrees with the observed dimensions of the jet.

Both of the ion-acceleration mechanisms studied above are connected with the excitation of strong plasma turbulence in the vicinity of the critical density. In this process the intensity of the scattered radiation should increase and its spectrum should broaden into both the red and blue sides. This agrees with the experimentally observed correlation between the appearance of a jet and the broadening of the spectrum and the increase in the intensity of the scattered radiation. The increase in the intensity of backscattering into

the focusing lens, which is recorded simultaneously with the appearance of a jet for $q \gtrsim 10^{14}$ W/cm^2, agrees with the theoretical ideas and experimental data on the role of double stimulated Mandel'shtam–Brillouin scattering processes arising in the presence of a reflected wave from the region of the critical plasma density.[2]

CONCLUSIONS

The method employed in this work to observe lateral scattering by plasma revealed two qualitatively different regimes of strong nonlinear interaction of the laser radiation with the plasma: the regime of self-focusing of the laser beam, corresponding to high energy fluxes and sharp focusing (small diameter of the laser beam on the surface of the target), and the regime of jet formation, when self-focusing of the laser beam does not occur, but rather strong turbulence is excited in the region of the critical density and beams of fast ions—jets—form. The proposed models make it possible to explain qualitatively the observed phenomena and agree with the results obtained by other authors.

We note that the observed sequence of regimes is characteristic for experiments with sharp focusing and a smooth distribution of the radiation intensity over the transverse cross section of the beam. This is what hinders the process of self-focusing and filamentation of the laser beam and why jet formation is observed. In experiments with laser-produced plasmas at high energies the light beams contain many small-scale intensity nonuniformities in the transverse cross section. Instead of the laser beam being focused as a whole, filamentation of the beam occurs. The threshold for this process is much lower than the threshold for self-focusing, since the scale size of the corona is determined by the diameter of the entire laser beam and not by a separate filament. The mechanism of jet formation can change correspondingly.

[1] O. Willi and P. T. Rumsby, Opt. Commun. **37**, 45 (1981).

[2] C. Joshi, C. E. Clayton, K. Marsh et al., ibid. **70**, 44 (1989).

[3] R. D. Jones, W. C. Mead, S. V. Coggeshall et al., Phys. Fluids **31**, 1249 (1988).

[4] G. Thiell and B. Meyer, Laser and Particle Beams **3**, 51 (1985).

[5] J. A. Stamper, R. H. Lehmberg, A. Schmitt et al., Phys. Fluids **28**, 2563 (1985).

[6] N. G. Basov, A. A. Gamaliĭ, A. E. Danilov et al., Pis'ma Zh. Eksp. Teor. Fiz. **38**, 60 (1983) [JETP Lett. **38**(2), 68 (1983)].

[7] B. Grek, F. Martin, T. W. Jonston et al., Phys. Rev. Lett. **41**, 1811 (1978).

[8] O. Willi, P. T. Rumsby, C. Hooker et al., Opt. Commun. **41**, 110 (1982).

[9] M. J. Herbst, J. A. Stamper, R. R. Whitlock et al., Phys. Rev. Lett. **46**, 328 (1981).

[10] V. L. Artsimovich, L. M. Gorbunov, and Yu. S. Kas'yanov, Zh. Eksp. Teor. Fiz. **89**, 2026 (1985) [Sov. Phys. JETP **62**(6), 1167 (1985)].

[11] V. L. Artsimovich, L. M. Gorbunov, Yu. S. Kas'yanov, and V. V. Korobkin, ibid. **80**, 1859 (1981) [Sov. Phys. JETP **53**(5), 963 (1981)].

[12] W. L. Kruer, Comm. Plasma Phys. Contr. Fusion **9**, 63 (1985).

[13] A. G. Litvak, V. A. Mironov, G. M. Frainman, and A. D. Yunakovskiĭ, Fiz. Plazmy **1**, 60 (1975) [Sov. J. Plasma Phys. **1**, 31 (1975).

[14] A. J. Schmitt, Phys. Fluids **31**, 3079 (1988).

[15] S. A. Akhmanov, A. P. Sukhorukov, and R. V. Khokhlov, Usp. Fiz. Nauk **93**, 19 (1967) [Sov. Phys. Usp. **10**, 609 (1967/1968)].

[16] A. B. Mikhaĭlovskiĭ, Theory of Plasma Instabilities [in Russian], Atomizdat, Moscow (1970), Vol. 1.

[17] B. B. Kadomtsev, in Reviews of Plasma Physics, Consultants Bureau, Vol. 4.

[18] V. Yu. Buchenkov, V. P. Silin, and S. A. Urypin, Phys. Rep. **164**, 120 (1988).

[19] A. A. Galeev, G. Laval', T. O'Neil et al., Zh. Eksp. Teor Fiz. **65**, 973 (1973) [Sov. Phys. JETP **38**(3), 482 (1974)].

[20] N. E. Andreev, Yu. A. Zakharenkov, N. N. Zorev et al., ibid. **76**, 976

(1979) [Sov. Phys. JETP **49**(3), 492 (1979)].

[21] V. L. Ginzburg, *Propagation of Electromagnetic Waves in Plasma* [in Russian], Nauka, Moscow (1973).

[22] A. V. Gurevich and A. P. Meshcherkin, Zh. Eksp. Teor. Fiz. **80**, 1810 (1981) [Sov. Phys. JETP **53**(5), 37 (1981)].

[23] V. P. Silin and V. T. Tikhonchuk, Phys. Rep. **135**, 1 (1986).

[24] N. E. Andreev, V. P. Silin, and V. T. Tikhonchuk, Fiz. Plazmy **14**, 851 (1988) [Sov. J. Plasma Phys. **14**, 501 (1988)].

[25] A. A. Andreev, N. E. Andreev, A. N. Sutyagin, and V. T. Tikhonchuk, *ibid.* **15**, 944 (1989) [Sov. J. Plasma Phys. **15**, 546 (1989)].

Translated by M. E. Alferieff